Prediction of Changes in Cell-substrate Contact under Cyclic Substrate Deformation Using Cohesive Zone Modelling

J.P. McGarry, B.P. Murphy, P.E. McHugh

National University of Ireland, National Centre for Biomedical Engineering Science and the Department of Mechanical and Biomedical Engineering, Ireland
patrick.mcgarry@nuigalway.ie, bruce.Murphy@nuigalway.ie
peter.mchugh@nuigalway.ie

The goal of this study entails the development of computational models of *in vitro* procedures in order to obtain an enhanced understanding of the mechanisms underlying the response of adherent cells to mechanical stimuli. The well established phenomenon of cell alignment under conditions of cyclic substrate stretching is considered. Cell-substrate adhesion is modelled using cohesive zone formulations. Two-dimensional cohesive zone modelling of cyclic substrate stretching reveals a mechanism of cell debonding associated with the cyclic accumulation of viscoelastic strain. Cell alignment is investigated for two distinct modes of cyclic substrate deformation using three-dimensional cohesive zone modelling. It is found that the alignment of the cell-substrate contact areas corresponds to directions of cell alignment observed experimentally for both modes (Wang et al. (2001)).

1 Introduction

The *in vitro* reorientation of isolated cells under conditions of cyclic substrate stretching is widely reported in the literature; see, for example, Wang et al. (1995), Takemasa et al. (1998) and Neidlinger-Wilke et al. (2001). Such behavior is observed for a variety of cell phenotypes including fibroblasts, human melanocytes and endothelial cells. Wang et al. (2001) report that under uniaxial substrate stretching, where substrate contraction is prohibited, cells were found to align at 90° to the direction of stretching. In cases where lateral substrate contraction was permitted cells were found to align at 65° to the direction of stretching. Both alignment directions correspond to the direction of minimum substrate strain. However, it is not clear from such *in vitro* studies why such cell reorientation occurs. In the current study computational models are developed in order to elucidate the mechanisms underlying such behavior. Two cohesive zone models are considered for modeling of cell-substrate adhesion (Beltz and Rice (1991), Xu and Needleman (1993)). Cells are modeled as

a viscoelastic continuum. Such an approach to cell modeling has been shown by Leipzig and Athanasiou (2004) to provide better predictions for initial creep response than the alternative bi-phasic modeling approach. Viscoelastic properties are fitted to the experimental measurements of Sato et al. (1990) for porcine endothelial cells.

2 Constitutive Relations

For elasticity, a hyperelastic description is used, where the stress can be derived from a strain energy density potential. A neo-Hookean description is adopted. In this case the form of the strain energy density potential, U, is

$$U = C_{10}(\bar{I}_1 - 3) + \frac{1}{D_1}(J-1)^2, \quad \bar{I}_1 = \bar{\lambda}_1^2 + \bar{\lambda}_2^2 + \bar{\lambda}_3^2, \tag{1}$$

where C_{10} and D_1 are material constants and J is the Jacobian of the deformation, $J = \det \mathbf{F}$. In the above, the $\bar{\lambda}_i$ are the principal deviatoric stretches, given by $\bar{\lambda}_i = J^{-\frac{1}{3}}\lambda_i$, where λ_i are the principal stretches of the deformation, which can be determined directly from the deformation gradient $\mathbf{F}$ as the eigenvalues of $\mathbf{F}^T \cdot \mathbf{F}$. The neo-Hookean description of hyperelasticity is chosen since it is a relatively straightforward representation of finite strain elasticity that can be specified in terms of two material constants C_{10} and D_1, that can easily be related to the initial or linear isotropic elastic constants, the elastic modulus E and Poisson's ratio ν. In specific terms, we use the relationships

$$C_{10} = \frac{E}{4(1+\nu)}, \quad D_1 = \frac{6(1-2\nu)}{E}. \tag{2}$$

The finite strain viscoelasticity used in this work is a generalization of small strain theory, and the basic formulation is most easily outlined beginning with the small strain theory. The viscoelastic material model. relates a time-varying shear strain, $\gamma(t)$, to shear stress, $\tau(t)$, by

$$\tau(t) = G_0 \int_0^t g_R(t-s)\,\dot{\gamma}(s)\,\mathrm{d}s \tag{3}$$

where $\dot{\gamma}(t)$ is the shear strain rate and the shear relaxation modulus, $g_R(t)$, is defined as

$$g_R(t) = \frac{G_R(t)}{G_0}, \tag{4}$$

$G_0 = G_R(0)$ being the instantaneous shear modulus and $G_R(t)$ the shear modulus at time t. It is assumed that the shear relaxation modulus is defined by a Prony series expansion such that

$$g_R(t) = 1 - \sum_{i=1}^{N} \overline{g}_i^p \left(1 - e^{-t/\tau_i^G}\right), \tag{5}$$

where $\overline{g}_i^p$ and τ_i^G are material constants and N is the number of terms in the Prony series (ABAQUS/Standard Users Manual, 2002; Hibbitt et al. (2002)). Equation (4) can be transformed by using integration by parts to yield

$$\tau\left(t\right) = G_0\left(\gamma - \int_0^t \dot{g}_R\left(s\right)\gamma\left(t-s\right)\mathrm{d}s\right) = \tau_0(t) - \int_0^t \dot{g}_R\left(s\right)\tau_0\left(t-s\right)\mathrm{d}s, \quad (6)$$

where $\tau_0(t) = G_0\gamma$ is the instantaneous shear stress at time t. Where volumetric deformation of the viscoelastic material is also being considered the following expression, analogous to eq. (6), is used to define the pressure

$$p\left(t\right) = -K_0\left(e^v - \int_0^t \dot{k}_R\left(s\right)e^v\left(t-s\right)\mathrm{d}s\right) = p_0(t) + \int_0^t \dot{k}_R\left(s\right)p_0\left(t-s\right)\mathrm{d}s, \quad (7)$$

where e^v is the volumetric strain, k_R is the bulk relaxation modulus, K_0 is the instantaneous bulk modulus and $p_0(t)$ is the instantaneous pressure at time t. As in eq. (5), k_R is represented using a Prony series

$$k_R\left(t\right) = 1 - \sum_{i=1}^{N}\overline{k}_i^p\left(1 - e^{-t/\tau_i^K}\right), \quad (8)$$

where $\overline{k}_i^p$ and τ_i^K are material constants and N is the number of terms in the Prony series. In ABAQUS it is assumed that $\tau_i^K = \tau_i^G$.

From this a generalization to finite strains can be made where the small strain elastic constitutive laws $\tau_0(t) = G_0\gamma$ and $p_0(t) = -K_0e^v$, involving the infinitesimal stresses $\tau_0(t)$ and $p_0(t)$, can be replaced with an appropriate finite strain constitutive law and an appropriate finite strain stress measure. In ABAQUS a generalization based on the expression

$$\begin{aligned}\boldsymbol{\tau}\left(t\right) = \ & \boldsymbol{\tau}_0(t) - \int_0^t \dot{g}_R\left(s\right)\mathbf{F}_t^{-1}(t-s)\cdot\boldsymbol{\tau}_0^D\left(t-s\right)\cdot\mathbf{F}_t(t-s)\mathrm{d}s \\ & - \int_0^t \dot{k}_R\left(s\right)\mathbf{F}_t^{-1}(t-s)\cdot\boldsymbol{\tau}_0^H\left(t-s\right)\cdot\mathbf{F}_t(t-s)\mathrm{d}s \end{aligned} \quad (9)$$

with

$$\boldsymbol{\tau}(t) = J\boldsymbol{\sigma}(t), \quad \boldsymbol{\tau}_0(t) = J\boldsymbol{\sigma}_0(t) = \boldsymbol{\tau}_0^D\left(t\right) + \boldsymbol{\tau}_0^H\left(t\right), \quad (10)$$

is used, where $\boldsymbol{\tau}(t)$ is the Kirchhoff stress tensor and $\boldsymbol{\tau}_0(t)$ is the instantaneous or elastic Kirchhoff stress that is decomposed into deviatoric, $\boldsymbol{\tau}_0^D(t)$, and volumetric, $\boldsymbol{\tau}_0^H(t)$, parts. In eq. (9) the transformation to finite strain necessitates the introduction of a relative deformation gradient tensor $\mathbf{F}_t$ that represents the deformation from the configuration at time $t - s$ to the configuration at

time t. In using this constitutive law, the Cauchy stress $\boldsymbol{\sigma}$ can be recovered by the determination of $\boldsymbol{\tau}$ through eq. (9) and the inversion of eq. $(10)_1$, and in a similar fashion the instantaneous or elastic Cauchy stress can be determined by $\boldsymbol{\sigma}_0(t) = \boldsymbol{\tau}_0(t)/J$ (Belytschko et al. (2000), Hibbitt et al. (2002)).

Finite strain viscoelasticity as described above is used in this study to represent the cell material behavior and, as is the case for material elasticity, much experimental work has been performed to determine values for cell viscoelastic material properties. The cells are therefore represented by both hyperelasticity and viscoelasticity and as such could be described as hyperviscoelastic. The formal linkage between the two constitutive descriptions is achieved by using hyperelasticity to specify the hyperelastic Cauchy stress at any time in the deformation history (any time t). This can then be identified as $\boldsymbol{\sigma}_0(t)$ and inserted into eqs (9) and (10) to determine the final stress ($\boldsymbol{\tau}(t)$ and hence $\boldsymbol{\sigma}(t)$) at time t due to both hyperelastic and viscous modes of deformation.

The cell substrate interface is described using cohesive zone models where by the energy of separation of two surfaces is expressed as a potential function, $\phi(\boldsymbol{\Delta})$, where $\boldsymbol{\Delta}$ is a vector of displacement jumps between the surfaces. Interface traction-separation relationships can be derived from the potential whereby

$$\mathbf{T} = \frac{\partial \phi\left(\boldsymbol{\Delta}\right)}{\partial \boldsymbol{\Delta}}, \tag{11}$$

where $\mathbf{T}$ is a vector of interface tractions. Two potential functions are considered in this study, the Xu-Needleman potential (12) and the Beltz-Rice potential (13), respectively

$$\begin{aligned}\phi\left(\Delta_n, \Delta_t\right) = \phi_n + \phi_n \exp\left(-\frac{\Delta_n}{\delta_n}\right) \\ \times \left\{\left[1 + \frac{\Delta_n}{\delta_n}\right](q-1) - \left[q + q\frac{\Delta_n}{\delta_n}\right]\exp\left(-\frac{\Delta_t^2}{\delta_t^2}\right)\right\},\end{aligned} \tag{12}$$

$$\begin{aligned}\phi\left(\Delta_n, \Delta_t\right) = \phi_n + \phi_n \exp\left(-\frac{\Delta_n}{\delta_n}\right) \\ \times \left\{\left[q + q\frac{\Delta_n}{\delta_n}\right]\sin^2\left(\frac{\pi \Delta_t}{\delta_t}\right) - \left[1 + \frac{\Delta_n}{\delta_n}\right]\right\},\end{aligned} \tag{13}$$

with

$$q = \frac{\phi_t}{\phi_n}, \tag{14}$$

where ϕ_n is the work of normal separation and ϕ_t is the work of tangential separation, Δ_n and Δ_t are the normal and tangential displacement jumps, respectively, across the interface, and δ_n and δ_t are normal and tangential characteristic lengths for the interface. Both cohesive zone models exhibit

an exponential form of the traction-separation relationship in the normal direction. This is consistent with the form of the force-separation curve measured for isolated ligand-receptor bonds (Leckband and Israelachvili (2001)). However, different forms are exhibited in the tangential direction, with the Xu-Needleman potential again yielding an exponential traction-separation relationship and the Beltz-Rice potential yields a sinusoidal relationship. While the former probably represents a more realistic representation of the localized breaking of ligand-receptor bonds in the tangential direction, the latter allows for cell re-adhesion in regions remote from the original bonding sites. Equations (13) and (14) can be generalized to three dimensions by the substitution:

$$\Delta_t = \left(\Delta_m^2 + \Delta_s^2\right)^{1/2}, \tag{15}$$

where Δ_s, Δ_m and Δ_n form a right-handed set.

3 Finite Element Model

A two-dimensional finite element model of a generic cell and substrate is shown in Fig. 1. By manipulation of symmetry only half the cell geometry is modelled. Displacement boundary conditions are applied to the right-hand side of the substrate such that the substrate strain varies cyclically from 0% strain to 5% strain at a frequency of 1 Hz. The cell material is assumed to be incompressible with an elastic modulus of 5 kPa, an elastic modulus of 2.5 MPa and a Poisson's ratio of 0.4 are used to model the silicone substrate. A coarser mesh is used for the substrate since it is several orders of magnitude stiffer than the cell and would consequently exhibit very low gradients of strain. A cell of height 15 μm and of contact radius 8.57 μm is shown in Fig. 1. However, several cell heights and contact radii are considered in this study.

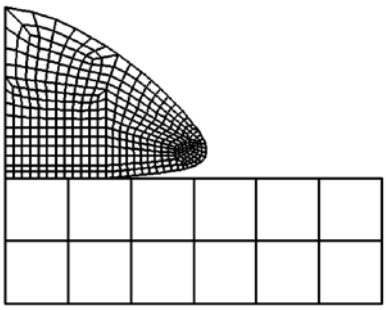

Fig. 1. Two-dimensional finite element cell-substrate model. The densely meshed section represents a cell attached to a coarsely meshed substrate. Cyclic strain is applied to the right-hand-side of the model in the horizontal direction.

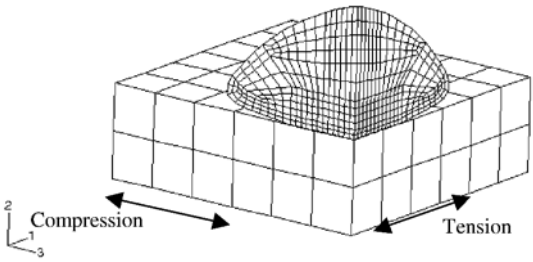

Fig. 2. Three-dimensional finite element cell-substrate model. The model is shown with the two planes of symmetry facing forwards.

By rotation of the two-dimensional cell geometry about its axis of symmetry a generic three-dimensional cell geometry is generated, as shown in Fig. 2. Again, by manipulation of symmetry only a quarter of the cell is modelled. Cyclic stretching of the substrate in the 1-direction is accompanied by cyclic compression of the substrate in the 3-direction due to the Poisson's effect. This is referred to as biaxial substrate deformation. Simulations are also performed in which lateral compression of the substrate is restrained. This is referred to as uniaxial substrate deformation. Both modes of deformation were used in the *in vitro* studies of cell reorientation by Wang et al. (2001).

4 Results

A brief summary of the main findings for two-dimensional and three-dimensional simulations is presented in this section. Interface strengths in the range of 500 Pa to 1000 Pa are used. This corresponds to a range of ligand-receptor bond strengths of 10 pN to 20 pN assuming a bond density of 50 sites/μm^2 (Thoumine et al. (1999)). Characteristic interface lengths of 25 nN are used in all simulations, based on experimentally measured ligand-receptor bond lengths.

Simulations are performed using a two-dimensional Xu-Needleman cohesive zone model. Following five cycles a tensile strain concentration develops above the cell-substrate contact opening as a result of cell viscoelasticity (see Fig. 3). This has the effect of lifting the cell from the substrate. Following 200 cycles the increasing magnitude of the tensile strain concentration results in debonding of a large section of the cell from the substrate. An equilibrium configuration is obtained following 200 cycles with no further debonding being computed. Quantitatively similar results are computed using the Beltz-Rice cohesive zone model.

As mentioned above, the cell geometry used is representative of a range of adherent cell types. Endothelial cells spread on a substrate can have heights

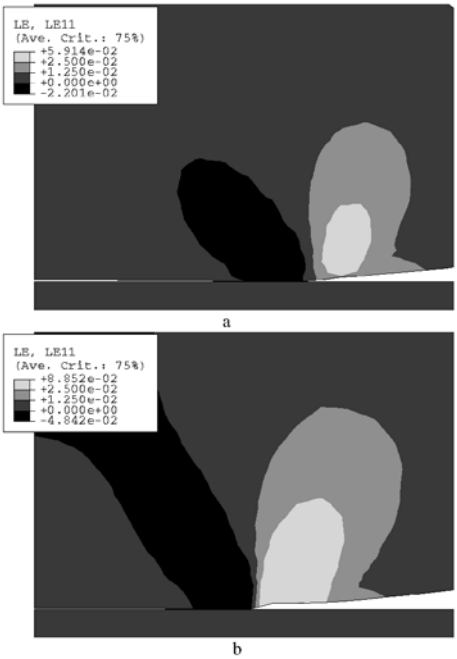

Fig. 3. Contours of strain component parallel to stretching direction computed using a two-dimensional Xu-Needleman model. Contour plots of the strain component parallel to the direction of substrate stretching are shown following five cycles and 200 cycles in Figs 3a and 3b respectively, Fig. 3b shows an increased zone of debonding.

as low as 5 μm (Davies et al. (1993)). In order to examine the influence of cell geometry on the mechanism of cell debonding models of spread cells of height 5 μm, with the entire cell base initially in contact with the substrate, are used. The debonded cell configuration is shown in Fig. 4a and Fig. 4b for cells with initial contact lengths of 8.5 μm and 12 μm, respectively. The mechanism of nodal debonding again entails the accumulation of a tensile strain concentration above the contact edge. While substantially more debonding occurs for the cell with a contact length of 12 μm the final contact length is very similar for both cases. However, it should be noted that for higher values of interface strength no debonding occurs for the cell with the lower contact length. In the case of the cell with a contact length of 12 μm a linear dependence of debonding on the interface strength is computed. In both cases the final contact length is very similar to that computed for the cell geometry shown in Fig. 1.

While two-dimensional models are used to investigate the mechanism of cell debonding, three-dimensional models must be used in order to investigate alignment of the cell substrate contact area. Strain contours for the case of

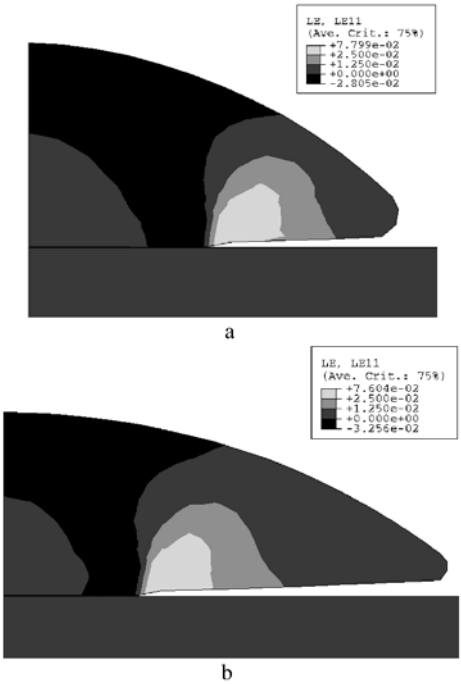

Fig. 4. Strain contours plotted on debonded cell geometry for cells of height 5 μm and radii of 8.5 μm (see Fig. 4a) and 12 μm (see Fig. 4b).

biaxial substrate deformation, where lateral contraction of the substrate due to the Poisson's effect occurs, are shown in Fig. 5. Contours of the strain component in the direction of substrate stretching are in Fig. 5a. As was revealed by two-dimensional models, the accumulation of tensile strain above the contact edge results in cell debonding in the direction of substrate stretching. Contours of the strain component in the direction of substrate contraction (Fig. 5b) reveal that a compressive strain accumulates above the contact edge, resulting in an upwards buckling of the cell. This leads to a small amount of cell debonding in the direction of substrate compression in the case of biaxial substrate deformation. In the case of uniaxial substrate deformation, where no lateral substrate deformation occurs, such an accumulation of compressive strain does not occur, with debonding being computed only in the direction of substrate stretching. The resultant contact areas for the case of biaxial and uniaxial substrate deformation are shown in Fig. 6a and Fig. 6b, respectively. Debonding in the compressive direction in the former case results in an alignment of the contact at 65° to the direction of stretching. In the case of uniaxial deformation, the contact area aligns perpendicular to the direction of substrate stretching. This complies with the directions of cell orientation observed *in vitro* by Wang et al. (2001) for such modes of substrate deformation.

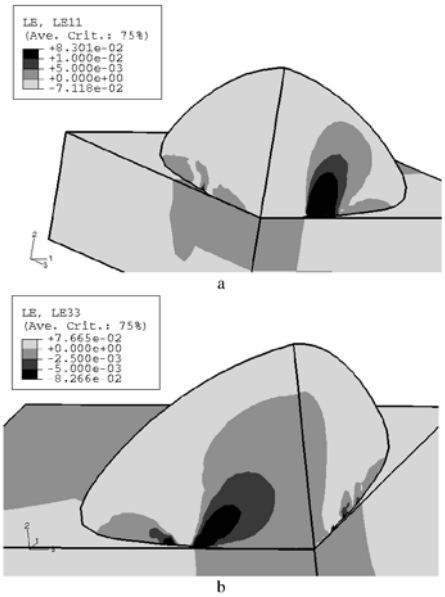

Fig. 5. Strain components in the direction of substrate stretching (see Fig. 5a), and substrate contraction (see Fig. 5b) for biaxial substrate deformation.

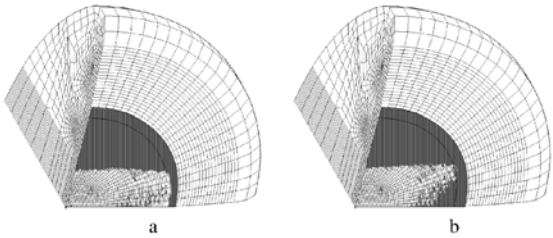

Fig. 6. Final cell-substrate contact areas: uniaxial substrate deformation (see Fig. 6a); biaxial substrate deformation (see Fig. 6b).

5 Discussion

A mechanism of cell debonding under cyclic substrate stretching where the accumulation of tensile strains due to cell viscoelasticity results in a lifting of the cell from the substrate is revealed by the computational models. The mechanism is shown to apply to a range of cell geometries. Development of compressive strain concentrations under biaxial substrate stretching results in a contact area alignment at 65° to the direction of stretching. The absence of such compressive strains in the case of uniaxial substrate stretching results in an alignment of the contact area perpendicular to the direction of stretching.

This complies with the directions of cell orientation observed *in vitro* by Wang et al. (2001) for such modes of substrate deformation. It should be noted that no significant alignment of the cell shape is computed by the computational models. This suggests that the computed breaking of cell-substrate adhesions acts as an initial step in the process of cell alignment. The associated unanchoring and subsequent rearrangement of the cell cytoskeleton has been shown to occur during cell alignment (Wang (2000)).

Acknowledgements. This research was supported by the Higher Education Authority of Ireland. Simulations were performed using the finite element code ABAQUS under and academic license from HKS Inc.

References

Beltz, G. E., and Rice, J. R. (1991). Dislocation nucleation versus cleavage decohesion at crack tips. In Lowe, T. C., Rollett, A. D., Follansbee, P. S., and Daehn, G. S., eds., *Modelling the Deformation of Crystalline Solids.* Warrendale, PA, USA: Proceedings TMS–AIME. 457–480.

Belytschko, T., Liu, W. K., and Moran, B. (2000). *Nonlinear Finite Elements for Continua and Structures.* New York: John Wiley and Sons.

Davies, P. F., Robotewskyj, A., and Griem, M. L. (1993). Endothelial cell adhesion in real time. *J. Clin. Invest.* 91:2640–2652.

Hibbitt, Karlsson, and Sorensen., eds. (2002). *ABAQUS/Standard User's Manual, Version 6.3.* Pawtucket, USA: Hibbitt, Karlsson and Sorensen, Inc. (HKS).

Leckband, D., and Israelachvili, J. (2001). Intermolecular forces in biology. *Quart. Rev. Biophys.* 34:105–267.

Leipzig, N. C., and Athanasiou, K. A. (2004). Unconfined creep compression of chondrocytes. *J. Biomech.* in press.

Neidlinger-Wilke, C., Grood, E. S., Wang, J. H.-C., Brand, R. A., and Claes, L. (2001). Cell alignment is induced by cyclic changes in cell length: studies of cells grown in cyclically stretched substrates. *J. Orthop. Res.* 19:286–293.

Sato, M., Theret, D. P., Wheeler, L. T., Ohshima, N., and Nerem, R. M. (1990). Application of the micropipette technique to the measurement of cultured porcine aortic endothelial cell viscoelastic properties. *J. Biomech. Eng.* 112:263–268.

Takemasa, T., Yamaguchi, T., Yamamoto, Y., Sugimoto, K., and Yamashita, K. (1998). Oblique alignment of stress fibers in cells reduces the mechanical stress in cyclically deforming fields. *Eur. J. Cell Biol.* 77:91–99.

Thoumine, O., Cardoso, O., and Meister, J.-J. (1999). Changes in the mechanical properties of fibroblasts during spreading: a micromanipulation study. *Eur. Biophys.* 28:222–234.

Wang, J. H.-C., Ip, W., Boissy, R., and Grood, E. S. (1995). Cell orientation response to cyclically deformed substrates: Experimental validation of a cell model. *J. Biomech.* 28:1543–1552.

Wang, J. H.-C., Goldschmidt-Clermont, P., Willie, J., and Yin, F. C.-P. (2001). Specificity of endothelial cell reorientation in response to cyclic mechanical stretching. *J. Biomech.* 34:1563–1572.

Wang, J. H.-C. (2000). Substrate deformation determined actin cytoskeleton reorganization: A mathematical modelling and experimental study. *J. Theor. Biol.* 202:33–41.

Xu, X.-P., and Needleman, A. (1993). Void nucleation by inclusion debonding in crystal matrix. *Model. Simul. Mater. Sci. Eng.* 1:111–132.